Application of Bragg-confined semiconductor structures for higher-energy resonant intersubband second-harmonic generation

D. Indjin,* V. Milanović, and Z. Ikonić
Faculty of Electrical Engineering, University of Belgrade, Bulevar Revolucije 73, 11000 Belgrade, Yugoslavia
(Received 20 May 1996)

The existence of bound electron states above the barrier in Bragg-confined structures is proposed as a means of extending the range of photon energies suitable for resonant intersubband second-harmonic generation beyond what is available in conventional quantum-well structures. Within the envelope-function approximation the expressions are first derived for energies and wave functions of bound states in Bragg structures with an asymmetric perturbation layer. A systematic procedure, based on supersymmetric quantum mechanics, is then described for the design of optimized structures to get the maximum nonlinear susceptibility. An example of a calculation for the case of pump photon energy $\hbar\omega \approx 240$ meV is also presented and the design aspects of such structures are considered. [S0163-1829(97)00115-X]

I. INTRODUCTION

Among various electronic and optical properties of low-dimensional semiconductor structures, their nonlinear optical properties attract continuous research attention because the nonlinearity can be resonantly enhanced by appropriate tailoring of the structure. The second-order nonlinearity based on intersubband transitions, responsible, e.g., for the second-harmonic generation (SHG) in the infrared, is most effective in the case of double resonance,[1] when the spacing between three equidistant states coincides with the pump photon energy. It has been studied in various asymmetric quantum well (QW) structures.[1–4] Values of the conduction-band offset (the barrier height) between the QW constituent semiconductors essentially set the upper limit of photon energies that can undergo frequency doubling under double-resonance conditions. This is because the QW has to accommodate three bound states and the band offset has to be typically 2.5–3 times larger than the pump photon energy. Indeed, though not for this reason alone, this process been studied mostly for the case of a 10.6-μm CO_2 laser pump[1–4] or larger wavelengths.[5] Pairs of semiconductors that have larger band offsets, suitable for QW's for higher-energy SHG, are often lattice mismatched or indirect-gap materials, which are inconvenient for this purpose.

The recently proposed Bragg-confined structures[6–11] (BCS's) that support bound states above the barrier top provide an effectively increased band offset and therefore may extend the applicability of QW's for resonant SHG at higher energies. A BCS is actually a semiconductor superlattice (SL) with the strict periodicity perturbed in a limited region, which may be called the perturbation layer. Along with the conventional ''piecewise continuous'' miniband spectrum, there appears an additional discrete spectrum: bound states lying in minigaps, at energies that are both below and above the top of the barriers. Their wave functions are localized to the perturbation layer, decaying away from it, as a result of constructive interference of waves reflected at well/barrier interfaces in the SL portions of the structure. All studies of BCS's until now considered only the case of a symmetric perturbation layer when the structure lacks any significant second-order nonlinearity.

In this paper we consider the possibility of using BCS's with an asymmetric perturbation layer for resonant intersubband SHG, taking advantage of the high-lying bound states they support. We first derive the expression for bound-state energies in such structures, allowing for an arbitrary variation of the potential and the effective mass in the perturbation layer. Then we turn to optimizing the structure with respect to the second-order nonlinearity, using a systematic procedure based on the supersymmetric quantum-mechanics approach.[12] Finally, we present an example of a calculation and a design of a structure matched for SHG of 5.1-μm (CO laser) radiation, also discussing the possibility of its practical realization.

II. THEORETICAL CONSIDERATIONS

In semiconductor microstructures the effective mass is generally position dependent (either in a continuous or a piecewise-constant manner) and the envelope function Schrödinger equation then takes the form[13]

$$-\frac{\hbar^2}{2}\frac{d}{dz}\left(\frac{1}{m(z)}\frac{d\Psi}{dz}\right)+U(z)\Psi=E\Psi. \tag{1}$$

Consider a one-dimensional SL structure having symmetric $U(z)$ and $m(z)$ dependences within a period d, perturbed by a single asymmetric perturbation layer of width δ [Fig. 1(a)]. While the strict periodicity of the structure is lost, there clearly remains ''local'' periodicity in the regions $(-\infty,-\delta)$ and $(\delta,+\infty)$, provided the long-range effects of the perturbation layer (e.g., the accumulated space charge) are neglected. In this case [exemplified in Fig. 1(b) for the Kronig-Penney SL] the wave function in the unperturbed regions may be written as a linear combination of two counterpropagating waves

$$\Psi(z)=C_1u_k(z)e^{ik_zz}+C_2u_{-k}(z)e^{-ik_zz}, \quad z<-\delta \text{ or } z>\delta, \tag{2}$$

where $u_{\pm k}(z)$ are the periodic parts of Bloch wave functions and k_z is the z component of the wave vector. To find the wave function in the unperturbed region one should first de-

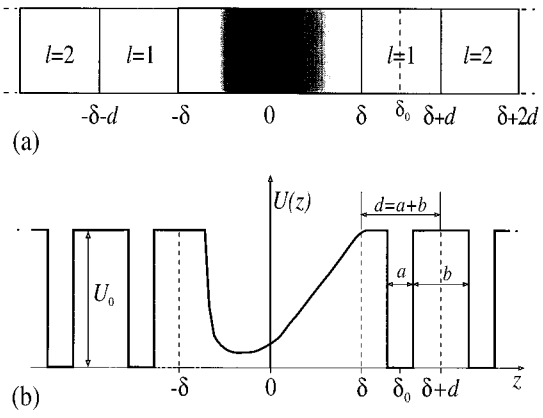

FIG. 1. (a) Schematic view of a periodic structure with an asymmetric perturbation layer and (b) the corresponding energy diagram in the case of Kronig-Penney SL portions of the structure.

termine $u_{\pm k}(z)$ within one period of the SL. Taking the period nearest the perturbation layer we have

$$u_{\pm k}(z)^{\pm ik_z z}=\text{const}[f_e(z)+\theta(\pm k_z)f_o(z)], \tag{3}$$

where $f_e(z)$ and $f_o(z)$ are the even and odd, with respect to the period midpoint at $z=\delta_0+d/2$, solutions of the Schrödinger equation (note that the Hamiltonian is symmetric with respect to this point). These are obtained by integrating Eq. (1) in the interval $(\delta,\delta+d)$ with the fundamental boundary conditions $f_e(\delta_0)=1$, $f_e'(\delta_0)=0$ and $f_o(\delta_0)=0$, $f_o'(\delta_0)=1$. The factor $\theta(\pm k_z)$ is determined from Bloch periodic boundary conditions $u_{\pm k}(\delta_0-d/2)=u_{\pm k}(\delta_0+d/2)$ as

$$\theta(\pm k_z)=i\left[\frac{f_e\left(\delta_0+\frac{d}{2}\right)}{f_o\left(\delta_0+\frac{d}{2}\right)}\right]\tan\left(\frac{\pm k_z d}{2}\right), \tag{4}$$

where $k_z d$ is given by the miniband dispersion relation $E(k_z)$, which reads[14]

$$\begin{aligned}\cos(k_z d)&=\frac{m_{\mathrm{SL}}(\delta_0)}{m_{\mathrm{SL}}\left(\delta_0+\frac{d}{2}\right)}\\&\quad\times[f_e(z)f_o'(z)+f_e'(z)f_o(z)]_{z=\delta_0+d/2}\\&\equiv F(E)\end{aligned} \tag{5}$$

because the effective mass $m_{\mathrm{SL}}(z)$ is position dependent.

To find bound states in minigaps, due to the presence of the perturbation, we recall that there k_z is complex, given by[15] $k_z=n\pi/d+ik_I$ in the nth minigap, with $k_I>0$. Equations (4) and (5) then become

$$\cosh(k_I d)=(-1)^n F(E) \tag{6}$$

and

$$\begin{aligned}\theta(\pm k_z)&=\pm\left\{-\left[\frac{f_e\left(\delta_0+\frac{d}{2}\right)}{f_o\left(\delta_0+\frac{d}{2}\right)}\right]\left[\frac{(-1)^n F(E)-1}{(-1)^n F(E)+1}\right]^{(-1)^n/2}\right\}\\&\equiv\pm\theta_{\mathrm{bound}}(E).\end{aligned} \tag{7}$$

With complex k_z the constant C_2 in Eq. (2) has to be zero in the region $(z>\delta)$ and the same applies to C_1 in $(z<-\delta)$. It follows from Eq. (3) that the wave function of a bound state in the nth minigap takes the following form in the lth period of the SL $[-\delta-ld<z<-\delta-(l-1)d$ or $\delta+(l-1)d<z<\delta+ld]$:

$$\Psi(z)=C_{L,R}(-1)^{n(l-1)}e^{-(l-1)k_I d}[f_e(z)\pm\theta_{\mathrm{bound}}f_o(z)], \tag{8}$$

where the subscript R and the plus sign correspond to $z>\delta$, while the subscript L and the minus sign correspond to $z<-\delta$, and it is implicitly taken that the functions $f_{e,o}$, initially defined within a single period (with $l=1$), map into more remote periods by simple translation. Inside the perturbation layer the wave function may also be written as a linear combination of two particular solutions

$$\Psi(z)=A_1y_1(z)+A_2y_2(z),\quad -\delta<z<\delta, \tag{9}$$

where $y_1(z)$ and $y_2(z)$ are found by integrating Eq. (1) using the fundamental boundary conditions $y_1(0)=1$, $y_1'(0)=0$ and $y_2(0)=0$, $y_2'(0)=1$. Imposing the conventional boundary conditions (the continuity of $\Psi(z)$ and of $[1/m(z)][d\Psi(z)/dz]$) at $z=\pm\delta$ to the wave functions (8) (with $l=1$) and (9) results in a 4×4 homogeneous linear system in A_1, A_2, C_L, and C_R. Nontrivial solutions require the corresponding determinant to be zero, which, together with $f_e(-\delta)=f_e(\delta)$, $f_e'(-\delta)=-f_e'(\delta)$, $f_o(-\delta)=-f_o(\delta)$, $f_o'(-\delta)=f_o'(\delta)$, and $m_{\mathrm{SL}}(-\delta)=m_{\mathrm{SL}}(\delta)$, results in

$$\begin{vmatrix}\eta(\delta) & 0 & -y_1(-\delta) & -y_2(-\delta)\\ -\frac{m_\delta(-\delta)}{m_{\mathrm{SL}}(\delta)}\eta'(\delta) & 0 & -y_1'(-\delta) & -y_2'(-\delta)\\ 0 & \eta(\delta) & -y_1(\delta) & -y_2(\delta)\\ 0 & \frac{m_\delta(\delta)}{m_{\mathrm{SL}}(\delta)}\eta'(\delta) & -y_1'(\delta) & -y_2'(\delta)\end{vmatrix}=0, \tag{10}$$

where $\eta(z)=f_e(z)+\theta_{\text{bound}}f_o(z)$ and $m_\delta(z)$ denotes the electron effective mass in the perturbation layer. From Eq. (10) the bound-state energies in SL's with a generally asymmetric perturbation layer are found from

$$
\begin{aligned}
&-\frac{m_\delta(-\delta)}{m_{\text{SL}}(\delta)}\eta'(\delta)\Big\{\eta(\delta)[y_1(-\delta)y_2'(\delta)-y_1'(\delta)y_2(-\delta)]\\
&\quad+\frac{m_\delta(\delta)}{m_{SL}(\delta)}\eta'(\delta)[y_1(\delta)y_2'(-\delta)-y_1(-\delta)y_2(-\delta)]\Big\}\\
&\quad-\eta(\delta)\Big\{\eta(\delta)[y_1'(-\delta)y_2(\delta)-y_1'(\delta)y_2'(-\delta)]\\
&\quad+\frac{m_\delta(\delta)}{m_{\text{SL}}(\delta)}\eta'(\delta)[y_1(\delta)y_2'(-\delta)-y_1'(-\delta)y_2(\delta)]\Big\}\\
&=0. \qquad (11)
\end{aligned}
$$

The boundary conditions at $z=\pm\delta$ enable the three coefficients, e.g., $A_{1,2}$ and C_L, to be expressed in terms of C_R as

$$
\begin{aligned}
A_{1,2}&=\left[\eta(\delta)y_{2,1}'(\delta)-\frac{m_\delta(\delta)}{m_{\text{SL}}(\delta)}\eta'(\delta)y_{2,1}(\delta)\right]\\
&\quad\times\frac{1}{W(y_1,y_2)|_{z=\delta}}C_R\equiv K_{1,2}C_R,\\
C_L&=\left[\frac{\eta(\delta)y_2'(\delta)-\frac{m_\delta(\delta)}{m_{\text{SL}}(\delta)}\eta'(\delta)y_2(\delta)}{\eta(\delta)y_2'(-\delta)+\frac{m_\delta(-\delta)}{m_{\text{SL}}(\delta)}\eta'(\delta)y_2(-\delta)}\right]\\
&\quad\times\frac{W(y_1,y_2)|_{z=-\delta}}{W(y_1,y_2)|_{z=\delta}}C_R\\
&\quad\equiv K_TC_R, \qquad (12)
\end{aligned}
$$

where $W(y_1,y_2)=y_1(z)y_2'(z)-y_1'(z)y_2(z)$ and C_R itself is determined from the wave-function normalization $\int_{-\infty}^{+\infty}|\Psi(z)|^2dz=1$. Using Eqs. (8) and (9) we find

$$
C_R=\left[\frac{(1+K_T^2)Q}{1-e^{-2k_Id}}+K_1^2Y_1+K_2^2Y_2+2K_1K_2Y_{12}\right]^{-1/2}, \qquad (13)
$$

where $Q=\int_\delta^{\delta+d}[f_e^2(z)+\theta_{\text{bound}}^2f_o^2(z)]dz$, $Y_{1,2}=\int_{-\delta}^{\delta}y_{1,2}^2(z)dz$, and $Y_{12}=\int_{-\delta}^{\delta}y_1(z)y_2(z)dz$.

This completes the procedure of finding the bound-state wave functions. In the special case of a symmetric perturbation layer the fundamental solutions inside it, $y_1(z)$ and $y_2(z)$, have even and odd parity, respectively, and the full wave function then also has a definite parity. Equation (11) would then take the form

$$
\begin{aligned}
&\left[\eta(\delta)y_1'(\delta)-\frac{m_\delta(\delta)}{m_{\text{SL}}(\delta)}\eta'(\delta)y_1(\delta)\right]\\
&\times\left[\eta(\delta)y_2'(\delta)-\frac{m_\delta(\delta)}{m_{\text{SL}}(\delta)}\eta'(\delta)y_2(\delta)\right]=0, \qquad (14)
\end{aligned}
$$

where the zeros of the first (second) term correspond to energies of even (odd) bound states of this symmetric structure.

For any general forms of the SL (symmetric) period and the (asymmetric) perturbation layer it is very likely that the above procedure would have to be performed numerically. The particular case of the rectangular (Kronig-Penney) SL, however, enables the functions $f_{e,o}(z)$ and the dispersion $E(k_z)$ to be found analytically.[13,16] This is the case one usually has in practice, or at least a good approximation to it, neglecting the self-consistency effects [Fig. 1(b)]. Numerical solution of the Schrödinger equation then has to be performed only in the perturbation layer $(-\delta,+\delta)$ to find $y_{1,2}(z)$.

The bound-state wave functions decay away from the perturbation layer, with the decay constant given by Eq. (6). They are derived from bound states (or resonant states) of the perturbation layer for energies below (above) the barrier top. The degree of the wave-function confinement (localization) reflects the degree of constructive interference of waves scattered at SL interfaces, as observed in the region of the perturbation layer. Good localization corresponds to large values of k_Id, which is difficult to maximize analytically for any general structure. Yet, for Kronig-Penney SL's the maximum localization conditions for above-the-barrier states are simple and completely analogous to those for optical multilayer structures.[17] They have the form of quantum-mechanical Bragg reflection conditions[6–11]

$$
k_Bb=(q+\tfrac{1}{2})\pi, \quad k_Wa=(r+\tfrac{1}{2})\pi, \qquad (15)
$$

where $k_B=[2m_B(E-U_0)/\hbar^2]^{1/2}$, $k_W=[2m_WE/\hbar^2]^{1/2}$, and $q,r=0,1,2,3,\ldots$ (m_B and m_W are the effective masses in the barrier and well in the SL portion of the structure). Equations (15) thus define the structure parameters necessary to get the best localization of some above-the-barrier state. Below-the-barrier states are generally well localized anyway and rather insensitive to the structure parameters, provided they do not come too close to allowed minibands of the SL.

Considering now the double-resonant SHG in these structures, we note that (at least) three equidistant levels are required for this process. The fact that BCS's support discrete states at above-the-barrier energies enables one to increase the pump (and harmonic) photon energies beyond the range provided by classical QW structures with all three states below the barrier. The pump light wavelength of $\lambda\approx5\,\mu$m, for instance, would require a classical QW with the band offset of $\geqslant0.6$ eV at least, in order to accommodate three states, which is the limit of availability in most heterojunctions. The problem may be solved by resorting to a BCS type of structure, with two states below and one above the barrier. Clearly, the wave functions of three equidistant states should be well localized so as to have a good overlap (otherwise the transition matrix elements will be small). As additional design guidelines, we note that energies of below-the-barrier states are mainly determined by the perturbation layer parameters, and much less by those of SL, and care should be taken only to keep them away from SL minibands. The energy of above-the-barrier state, on the other hand, is strongly influenced by both the perturbation layer and the SL parameters, as is its localization. As the third point, the Fermi level in an n-doped BCS will be close to the lowest miniband, so the lowest bound state has to be below it in order to acquire significant electron concentration. In view of all these constraints and the complicated form of Eq. (11), the design of a

more or less optimized structure of this type by a purely trial-and-error method would be very difficult. Instead, one may first attempt to design a symmetric structure with equidistant states, their energies given by a simpler Eq. (14). Being symmetric it would lack any second-order nonlinearity, but should satisfy all other requirements stated above. As the second step this symmetric BCS should be used as a starting point to generate a family of isospectral structures, which will be asymmetric and therefore allow SHG by using the supersymmetric quantum mechanics (SUSYQM) approach.[12] From this family the structure with the best performance is then selected.

In applying the above methods to real semiconductor structures, however, due attention is to be paid to the effects of nonparabolicity, which may be quite prominent because one deals with energies high above the conduction-band edge, at least in some parts of the structure. The nonparabolicity may be conveniently described by an energy-dependent effective mass, based on the two-band Kane model[18]

$$m^*(z,U(z),E)=m(z)\left[1+\frac{E-U(z)}{E_g(z)}\right], \tag{16}$$

where $E_g(z)$ is the material composition- (and hence the position-) dependent band gap. Using the standard SUSYQM approach necessitates that Eq. (1), with the energy- and position-dependent effective mass, should be recast into a more conventional form with a variable potential but constant mass. This can be accomplished by introducing a suitably chosen invertable coordinate transform $z=g(x)$ in Eq. (1), which then takes the form

$$-\frac{\hbar^2}{2\underline{m}g'^2}\frac{d^2u(x)}{dx^2}-\frac{\hbar^2}{2\underline{m}g'^2}\left\{-\frac{1}{4}\left[\frac{d}{dx}[\ln(\underline{m}g')]\right]^2+\frac{1}{2}\frac{d^2}{dx^2}[\ln(\underline{m}g')]\right\}u(x)+[\underline{U}(x)-E]u(x)=0, \tag{17}$$

where the scaled wave function $u(x)$ is related to the true wave function by $\underline{\Psi}(x)=\Psi(g(x))=\text{const}u(x)\sqrt{\underline{m}g'}$, and $\underline{m}(x)=m(g(x))$, $\underline{U}(x)=U(g(x))$, and $g'=dg(x)/dx$. To cast Eq. (17) into the common textbook form we set a constraint

$$\underline{m}g'^2=m_0>0, \tag{18}$$

where m_0 does not depend on x, which gives

$$-\frac{\hbar^2}{2m_0}\frac{d^2u(x)}{dx^2}+[\underline{U}_{\text{eff}}(x)-E]u(x)=0, \tag{19}$$

with

$$\underline{U}_{\text{eff}}(x)=\underline{U}(x)-\frac{\hbar^2}{2m_0}\left[-\frac{1}{4}\left(\frac{d}{dx}(\ln\sqrt{\underline{m}})\right)^2+\frac{1}{2}\frac{d^2}{dx^2}(\ln\sqrt{\underline{m}})\right]. \tag{20}$$

Equation (19) has the identical eigenspectrum to the original Eq. (1), but it has the constant effective mass and can be subjected to the standard isospectral supersymmetric transform. According to the SUSYQM theory,[12] the supersymmetric partner to the potential $\underline{U}_{\text{eff}}(x)$ is given by

$$\underline{U}_{\text{ss}}(x)=\underline{U}_{\text{eff}}(x)-\frac{\hbar^2}{m_0}\frac{d^2}{dx^2}\{\ln[\lambda+\underline{I}(x)]\}, \tag{21}$$

where $\underline{I}(x)=\int_{-\infty}^{x}\varphi_u^2(x)dx$ and $\varphi_u(x)$ denotes any bound-state-scaled wave function $u(x)$. Transforming back to the real-space coordinate z, we find, after a lengthy derivation, that the supersymmetric partner potential to $U(z)$ of Eq. (1) is

$$\begin{aligned}U_{\text{ss}}(z)=&\left\{U(z)-\frac{\hbar^2}{\sqrt{m^*(z,U(z),E)}}\frac{d}{dz}\right.\\&\left.\times\left[\frac{1}{\sqrt{m^*(z,U(z),E)}}\frac{d}{dz}\{\ln[\lambda+I(z)]\}\right]\right\}\\&-\frac{\hbar^2}{2}\left\{-\frac{1}{2[m^*(z,U(z),E)]^3}\left(\frac{dm^*(z,U(z),E)}{dz}\right)^2\right.\\&\left.+\frac{1}{4[m^*(z,U(z),E)]^2}\frac{d^2m^*(z,U(z),E)}{dz^2}\right\}+\frac{\hbar^2}{2}\\&\times\left\{-\frac{1}{2[m^*(z,U_{\text{ss}}(z),E)]^3}\left(\frac{dm^*(z,U_{\text{ss}}(z),E)}{dz}\right)^2\right.\\&\left.+\frac{1}{4[m^*(z,U_{\text{ss}}(z),E)]^2}\frac{d^2m^*(z,U_{\text{ss}}(z),E)}{dz^2}\right\}.\end{aligned} \tag{22}$$

Equation (22) is in fact a differential equation, to be solved for $U_{\text{ss}}(z)$. This complicated form occurs because of $m^*=m^*(z,U_{\text{ss}}(z),E)$. If the mass were constant, $U_{\text{ss}}(z)$ would be given by an explicit expression.[12] To a good approximation, however, the nonparabolicity at lower energies may be neglected, and at higher energies one may take $m^*(z,U_{\text{ss}}(z),E)\approx m^*(z,U(z),E)$, inducing cancellation of the last two terms in Eq. (22), which then becomes an explicit expression for $U_{\text{ss}}(z)$. Having derived the expression for $U_{\text{ss}}(z)$ using the coordinate transform and SUSYQM methods, all the relations hereafter will be given in terms of the real coordinate z only.

The explicit, though approximate, expression for $U_{\text{ss}}(z)$ should now be used in the Schrödinger equation

$$-\frac{\hbar^2}{2}\frac{d}{dz}\left(\frac{1}{m^*}\frac{d\Psi_{\text{ssi}}}{dz}\right)+U_{\text{ss}}(z)\Psi_{\text{ssi}}=E\Psi_{\text{ssi}}. \tag{23}$$

The corresponding wave functions, as they depend on the real coordinate z, are

$$\Psi_{\text{ssi}}(z)=\Psi_i(z)+\frac{\varphi(z)}{\lambda+I(z)}\int_z^{+\infty}\varphi(t)\Psi_i(t)dt, \tag{24}$$

where $\Psi_i(z)$ denotes the ith eigenfunction of Eq. (1), $\varphi(z)$ stands for any eigenfunction of Eq. (1) (usually, though not necessarily, that of the ground state), and

$$I(z)=\int_{-\infty}^{z}\varphi^2(t)dt. \tag{25}$$

There is a free parameter λ in Eqs. (21)–(25), which may be given any value except those in the range $-1<\lambda<0$ for physical reasons (continuity of the wave functions). There-

fore, a single-parameter family of potentials $U_{ss}(z;\lambda)$ is generated. Specifically, choosing $\varphi(z)=\Psi_l(z)$, the normalized wave function $\Psi_{ssi}(z)$ with the same index $i=l$ reads

$$\Psi_{ssl}(z)=\frac{\sqrt{\lambda(\lambda+1)}}{\lambda+I(z)}\Psi_l(z). \tag{26}$$

Furthermore, if the original potential and the effective mass are symmetric and the eigenfunctions have definite parity, then

$$I(z)=\int_{-\infty}^{0}\varphi^2(t)dt+\int_0^z\varphi^2(t)dt=\frac{1}{2}+\int_{-z}^{0}\varphi^2(t)dt$$

$$=1-\int_{-\infty}^{-z}\varphi^2(t)dt=1-I(-z), \tag{27}$$

wherefrom

$$U_{ss}(z;\lambda)=U_{ss}(-z,-(\lambda+1)) \tag{28}$$

and one can see that all physically different potentials $U_{ss}(z)$ may be generated by giving only positive values to λ. A negative λ would just deliver $U_{ss}(z)$ of the same shape, but reversed. Finally, we may note that $U_{ss}(z)$ becomes only marginally different from $U(z)$ as $\lambda\to+\infty$; therefore major effects are to be expected at smaller values of λ.

Thus, starting from the original potential $U(z)$ (corresponding to the symmetric structure), one finds, via the supersymmetric transform, a parameter-dependent family of asymmetric isospectral potentials and varies the parameter λ so as to maximize the second-order nonlinearity. Throughout this scanning over λ the states energies remain unchanged, while the wave functions, and hence the transition matrix elements, vary.

III. NUMERICAL RESULTS AND DISCUSSION

As an example here we attempt to design and optimize a BCS-based asymmetric structure for double-resonant SHG matched for the pump wavelength of 5.1 μm (i.e., $\hbar\omega=242$ meV), corresponding, e.g., to CO laser radiation. We consider an n-doped structure based on direct-gap semiconductors and assume that the band gap is sufficiently large so that interband transitions are negligible. The $\chi^{(2)}_{zzz}$ nonlinear susceptibility then arises only due to electronic intersubband transitions and is given by (e.g., Ref. 1)

$$\chi^{(2)}_{zzz}=\frac{e^3}{L_z\epsilon_0\hbar^2}\sum_l\sum_k\frac{1}{(2\omega+\Omega_{ik})-i\Gamma_{ki}}$$

$$\times\sum_l M_{ik}M_{kl}M_{li}\left[\frac{\rho_{ii}-\rho_{ll}}{\omega+\Omega_{il}-\Gamma_{li}}-\frac{\rho_{ll}-\rho_{kk}}{\omega-\Omega_{lk}-i\Gamma_{kl}}\right], \tag{29}$$

where M_{ij} are the dipole matrix elements, Ω_{ij} are the transition frequencies between states i and j, ρ_{ii} denotes the sheet density of electrons residing on state i, L_z is the length of the structure, Γ_{ij} is the off-diagonal relaxation rates, and ω is the frequency of the (pump) light wave. The largest value of $\chi^{(2)}_{zzz}$ is obtained in the double-resonance regime, i.e., when $\omega=\Omega_{01}=\Omega_{12}$ for states labeled as 0, 1, and 2 (here taken to be the lowest three), and is given by

$$\chi^{(2)}_{zzz\,\max}=\frac{e^3(\rho_{00}-\rho_{11})}{L_z\epsilon_0}\frac{M_{01}M_{12}M_{20}}{(\hbar\Gamma_2)^2}, \tag{30}$$

where Γ_2 is the (assumed common) off-diagonal relaxation rate and the off-resonant contributions of states other than 0, 1, and 2 are neglected. Variation of the potential and the wave functions by changing the parameter λ (Sec. II) will clearly affect the matrix elements in Eq. (30), but not the population of states, since all the potentials are isospectral. Assuming that Γ_2 remains (at least approximately) constant as λ varies, the optimization of $\chi^{(2)}_{zzz}$ amounts to finding the value of λ that will maximize the product of the three matrix elements $\Pi^{(2)}(\lambda)=M_{01}M_{12}M_{20}$. Certainly, the potential $U_{ss}(z)$ obtained by the procedure described in Sec. II should be practically realizable, i.e., the full potential excursion should not exceed the band offset offered by the semiconductor system used. In particular, the derivative of the effective mass, which appears in Eq. (22), implies that an abrupt change of the effective mass would lead to the optimized potential with δ-function peaks. The corresponding wave functions would still be regular and physically acceptable and could straightforwardly be used in further calculation. Yet the potential with δ-function peaks cannot be realized in practical semiconductor structures, so we prefer to avoid such a situation. It is thus clear that the structure should be designed so that the effective mass varies smoothly or, even better, is simply constant. The potential (i.e., the conduction-band edge) and the effective mass in any graded semiconductor alloy are related to each other to some extent, but still may be tailored independently within some limits, set by either physical constraints (no component of an alloy may contribute more than 100% or less than 0%) or additional requirements (e.g., that the structure should be unstrained or strained within reasonable limits). In this example we attempt to design a graded alloy structure such that its potential is variable but the effective mass constant (except for a slight z dependence coming in implicitly, through nonparabolicity). This additional restriction upon the effective mass is intended to make $U_{ss}(z)$ generally smoother. The possibility of achieving such a structure is considered next.

In composition-modulated (graded) ternary alloys such as $Al_xGa_{1-x}As$, both the conduction-band edge (i.e., the potential) and the effective mass are position dependent. However, the two dependences are related to each other and cannot be tailored separately. It is therefore not possible to achieve a specified constant effective mass and a specified variable potential unless the two semiconductors happen to have the same effective mass. The situation is thoroughly changed if we go to quaternary alloys. While they formally provide enough freedom to get any m^* and $U_{ss}(z)$, there are some practical restrictions to be observed. For one, the fact that any single compound cannot contribute more than 100% or less than 0% in the alloy composition significantly limits what really can be achieved. Furthermore, the variation of the alloy composition also leads to the lattice constant varying across the structure, which may be large enough to in

duce a considerable strain and appearance of misfit dislocations, which would degrade the device performance. Among binary III-V compounds there is no pair that is simultaneously lattice matched and effective mass matched while having a finite conduction-band offset, so that their graded alloy would automatically be strain-free and have a constant effective mass. However, such pairs can be found among alloys. Consider, for instance, a quaternary alloy of the type $A_xB_{1-x}C_yD_{1-y}$. We do the following two steps.

(i) Keeping the atomic species A,B,C,D fixed, we search for two different compositions, i.e., $A_{x_1}B_{1-x_1}C_{y_1}D_{1-y_1}$ and $A_{x_2}B_{1-x_2}C_{y_2}D_{1-y_2}$, where at least one of $x_1 \neq x_2$ and $y_1 \neq y_2$ is satisfied, which are characterized by the same lattice constant and effective mass and at the same time have as large a band offset U_0 as possible.

(ii) Then we make a graded alloy of the two ''basis'' alloys $(A_{x_1}B_{1-x_1}C_{y_1}D_{1-y_1})x' + (A_{x_2}B_{1-x_2}C_{y_2}D_{1-y_2})(1-x')$, where $x' = x'(z)$ is varied in such a way as to get the required modulation of the conduction-band edge, i.e., of the potential. This graded alloy will still be of the same quaternary $A_{x(z)}B_{1-x(z)}C_{y(z)}D_{1-y(z)}$ type as are the two basis alloys and the maximum excursion of $U(z)$ is clearly limited to U_0. If the atomic species in basis alloys were chosen differently, their graded alloy would be at least a quintarnary or more complicated alloy, which we prefer to avoid.

To describe this procedure in more detail, we first denote the two basis alloys $A_{x_1}B_{1-x_1}C_{y_1}D_{1-y_1}$ and $A_{x_2}B_{1-x_2}C_{y_2}D_{1-y_2}$ as $Q(x_1,y_1)$ and $Q(x_2,y_2)$, respectively. If two alloys are to have the same effective mass and lattice constant, the following two equations should be satisfied:

$$x_1y_1m_{AC}+x_1(1-y_1)m_{AD}+y_1(1-x_1)m_{BC}+(1-x_1)(1-y_1)m_{BD} = x_2y_2m_{AC}+x_2(1-y_2)m_{AD}+y_2(1-x_2)m_{BC}+(1-x_2)(1-y_2)m_{BD}, \tag{31}$$

$$x_1y_1a_{AC}+x_1(1-y_1)a_{AD}+y_1(1-x_1)a_{BC}+(1-x_1)(1-y_1)a_{BD} = x_2y_2a_{AC}+x_2(1-y_2)a_{AD}+y_2(1-x_2)a_{BC}+(1-x_2)(1-y_2)a_{BD}, \tag{32}$$

where m_{AC} and a_{AC} denote the effective mass and the lattice constant of the AC compound, etc., and these quantities in the alloy are taken to scale linearly with the contributions of the corresponding compounds (Vegard's law), themselves being tabulated in the literature. Certainly, this is only a good approximation to the true dependences of these quantities on the alloy composition. There are very few data on appropriate ''bowing'' parameters for various alloys, and if these could be found for the alloys considered here the procedure would remain essentially the same, with slight modification of Eqs. (31) and (32). Clearly, with two equations and four unknowns, the system is indeterminate. There may be a large number, i.e., a continuous set of solutions, but they should belong to the interval $0 \leqslant (x_1,x_2,y_1,y_2) \leqslant 1$ to be physically acceptable. Fixing some values of, e.g., x_1 and y_1 within this range, Eqs. (31) and (32) reduce to a quadratic equation in, say, x_2 and, upon solving it, a linear equation in y_2. However, of the two solutions one is trivial $x_2 = x_1$ and $y_2 = y_1$, so one should extract the nontrivial solution by using the Viete rules to get

$$x_2 = -\frac{y_1}{\mathcal{R}} - \frac{\mathcal{A}}{\mathcal{C}\mathcal{R}} - \frac{\mathcal{B}}{\mathcal{C}}, \tag{33}$$

$$y_2 = y_1 + \mathcal{R}(x_2 - x_1), \tag{34}$$

where

$$\mathcal{R} = \frac{\mathcal{A}\mathcal{F} - \mathcal{C}\mathcal{D}}{\mathcal{C}\mathcal{E} - \mathcal{F}\mathcal{B}} \tag{35}$$

and

$$\mathcal{A} = m_{AD} - m_{BD}, \quad \mathcal{B} = m_{BC} - m_{BD},$$
$$\mathcal{C} = m_{AC} - m_{AD} - m_{BC} + m_{BD}, \quad \mathcal{D} = a_{AD} - a_{BD},$$
$$\mathcal{E} = a_{BC} - a_{BD}, \quad \mathcal{F} = a_{AC} - a_{AD} - a_{BC} + a_{BD}. \tag{36}$$

Thus it should checked whether (x_2,y_2) found in this way are physically acceptable, while (x_1,y_1) take various values from the interval $[0,1]$ and determine the effective mass and the band offset, which will characterize the pair of alloys. Using the data for the effective mass and the lattice constant of III-V binary compounds,[19] where III denotes Al, Ga, or In and V denotes P, As, or Sb, we explored all the nine possible quaternary alloys based upon them. In six cases no acceptable solution (x_2,y_2) was found for any (x_1,y_1). In the rest of the three cases, the conduction-band offset U_0 was then calculated using the data of Ref. 20. It was found that the alloy $Al_xIn_{1-x}P_ySb_{1-y}$ offers the maximum U_0 of 231 meV, which is insufficient to accommodate three levels spaced by ~ 240 meV. In $Al_xIn_{1-x}P_yAs_{1-y}$ the best U_0 amounted to 360 meV, with the effective mass in the range ~ 0.15 (in free-electron mass units), while the alloy $Ga_xIn_{1-x}P_ySb_{1-y}$ had U_0 around 500 meV and the effective mass in the range ~ 0.07.

Since the supersymmetric transform is known to make the potentials generally ''deeper'' than the originals and the matrix element product $\Pi^{(2)}$ tends to increase as the effective mass decreases, we choose the alloy $Ga_xIn_{1-x}P_ySb_{1-y}$. Specifically, we choose the basis alloys $Q_1 = (x_1 = 0, y_1 = 1)$ and $Q_2 = (x_2 = 0.83, y_2 = 0.46)$, i.e., InP and $Ga_{0.83}In_{0.17}P_{0.46}Sb_{0.54}$, with the effective mass $m^* = 0.073$, the band offset $U_{0\max} = 580$ meV, and the band gaps of

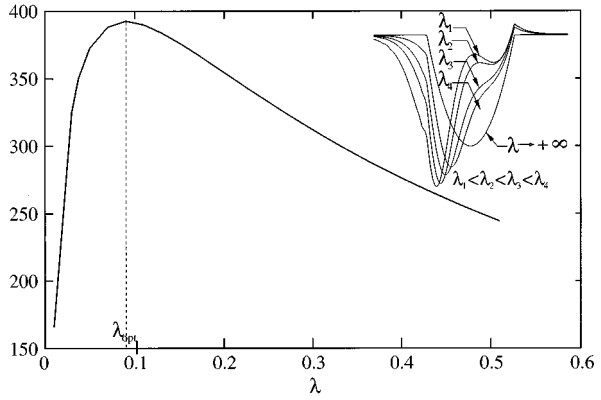

FIG. 2. Product of matrix elements $\Pi^{(2)}$ in the asymmetric BCS as it depends on the parameter λ in the supersymmetric transform, obtained with $\varphi(z)=\Psi_0(z)$.

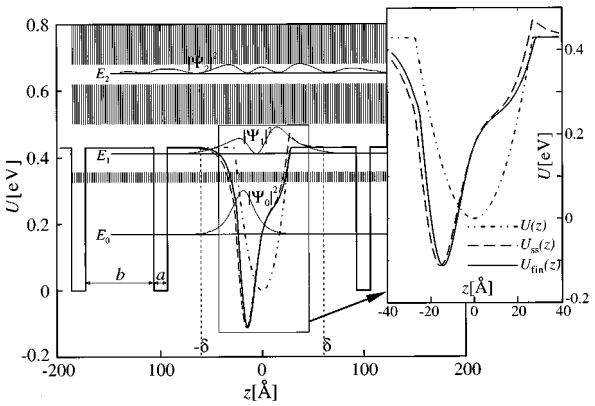

FIG. 3. Optimized supersymmetric potential $U_{ss}(z)$ (dashed line), the starting symmetric potential (dotted line), and the finally adjusted potential $U_{fin}(z)$ to be realized (solid line).

$E_{g1}=1.35$ eV and $E_{g2}=1.5$ eV. Both are direct-gap semiconductors, as may be seen directly or by linear interpolation of the data in Refs. 20 and 21.

The first step in the design is to generate a symmetric structure with three equidistant states, spaced by $\Delta E=\hbar\omega=242$ meV, observing all the restrictions discussed in Sec. II. We took the perturbation layer potential to be of truncated parabolic type

$$U(z)=\begin{cases} U_0, & -\delta<z<-z_0 \text{ or } z_0<z<\delta \\ \dfrac{1}{2}m^*\left(\dfrac{\Delta E}{\hbar}\right)^2 z^2, & -z_0<z<z_0, \end{cases} \tag{37}$$

where $z_0=(2U_0\hbar^2/m^*\Delta E^2)^{1/2}$ is the point where the parabolic potential reaches the value U_0, here taken to amount to $U_0=430$ meV. Energies of the two below-the-barrier bound states may be estimated from the ideal linear harmonic oscillator formula $E_i=(i+\frac{1}{2})\Delta E$, $i=0,1$. After a number of trials we found that the structure with $a=14$ Å, $b=66.5$ Å, and $2\delta=121$ Å, with the nonparabolicity included via Eq. (16) and $E_g(z)=[1-U(z)/U_{0\max}]E_{g1}+[U(z)/U_{0\max}]E_{g2}$, satisfies about all the requirements. It has bound states at $E_0=171$ meV (even state), $E_1=414$ meV (odd state), and $E_2=657$ meV (even state), which are either below the first miniband or deep inside minigaps between the minibands extending from 325 to 356 meV, 499 to 619 meV, and 680 to 896 meV. The first two bound states are below the barrier and are very well localized since E_0 is well below the first miniband and E_1 is close to the middle of the minigap. The third state is above the barrier, with the conditions (15) satisfied as $k_W(E_2)a=\pi/2$ and $k_B(E_2)b=3\pi/2$ (so it is optimally localized), and interlevel spacing is $\Delta E_{01}=\Delta E_{12}=243$ meV. This provides a good basis for the supersymmetric transform to be applied.

A problem that arises in this second step is that the energy-dependent effective mass leads to an energy-dependent supersymmetric potential, which will be different for the three states and cannot be realized in real structures. To circumvent this difficulty we made the supersymmetric transform while fixing the energy to the middle of the range of interest and subsequently did some ''fine polishing'' of the optimized potential. By changing the value of λ in Eqs. (24) and (26) and calculating the matrix elements $M_{ij}=\int_{-\infty}^{+\infty}\Psi_{ssi}^* z\Psi_{ssj}dz$, we found that the product $\Pi^{(2)}$ depends on λ as displayed in Fig. 2 [in the case $\varphi(z)=\Psi_0(z)$] and takes the maximum value of $\Pi^{(2)}_{\max}=392$ Å^3 at $\lambda_{opt}=0.09$. Mostly affected by the transform is the central part of the perturbation layer, which becomes remarkably asymmetric, while the SL portion of the structure remains essentially unchanged. The optimized potential and the original symmetric potential are given in Fig. 3. Bound-state energies were then calculated for this optimized potential according to Eq. (11) and values of $E_0=162$ meV, $E_1=418$ meV, and $E_2=654$ meV were found. The levels' equidistance condition was thus significantly perturbed, as a consequence of approximations introduced in the supersymmetric transform, with $\Delta E_{01}=256$ meV and $\Delta E_{12}=236$ meV instead of the target value $\Delta E=242$ meV. To correct for this it is necessary to modify $U_{ss}(z)$ slightly. Whatever law of modification is used, two free parameters are necessary to allow two goals ($\Delta E_{01}=242$ meV and $\Delta E_{12}=242$ meV) to be achieved. Clearly, this corrected potential should be as close to the original $U_{ss}(z)$ as possible, so that it still has a large (at least close to maximum) product of matrix elements $\Pi^{(2)}$. Here we have used simple coordinate scaling inside the perturbation layer only, i.e., instead of $U_{ss}(z)$ we set a new potential $U_{fin}(z')$, defined as $U_{fin}(z')=U_{ss}(z)$, where $z'=\alpha z+\beta|z|$ and α and β are the symmetric and asymmetric dilatation coefficients. These are to be adjusted by numerical solution of the Schrödinger equation. The small peak in $U_{ss}(z)$, on the right-hand side of the well (Fig. 3), was also eliminated by this method. The values of the dilatation coefficients $\alpha=1.02$ and $\beta=0.10$ were found to restore the levels' equidistance, giving $E_0=168$ meV, $E_1=411$ meV, and $E_2=653$ meV (hence $\Delta E_{01}=243$ meV and $\Delta E_{12}=242$ meV), and the product of matrix elements now is $\Pi^{(2)}=385$ Å^3. This final potential, also given in Fig. 3, is only slightly different from $U_{ss}(z)$ and the corresponding values of $\Pi^{(2)}$ are very close as well, i.e., the ''degree of asymmetry'' of the structure has not changed very much (note that $\alpha=1$ and $\beta=0$ make the ''identity transform'').

The final potential displayed in Fig. 3 can now be realized using the graded alloy $(Q_2)_{x'}(Q_1)_{1-x'}$ by suitably grading the ''mole fraction'' $x'(z)$. In effect

$$U_{0\max}x'(z)=U_{fin}(z)+\text{const}, \tag{38}$$

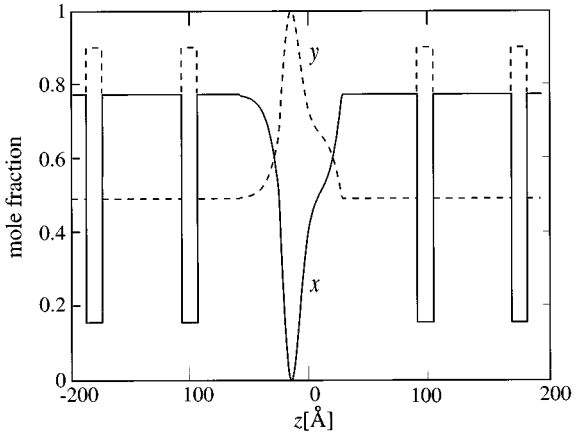

FIG. 4. Grading profile, i.e., the mole fractions $x(z)$ and $y(z)$ in the $Ga_xIn_{1-x}P_ySb_{1-y}$ alloy, necessary to realize the potential $U_{\rm fin}(z)$ in Fig. 3.

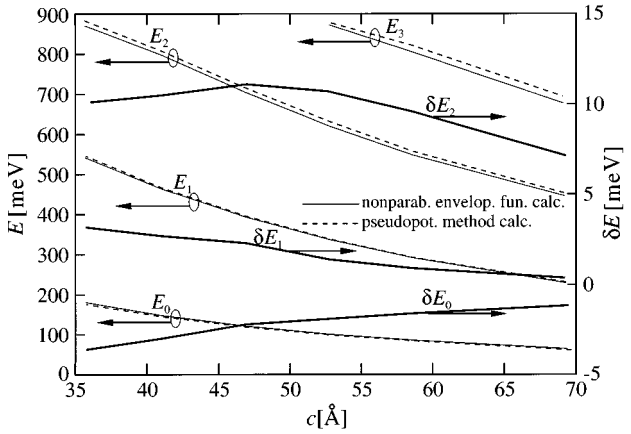

FIG. 5. Bound-state energies in $Ga_{0.83}In_{0.17}P_{0.46}Sb_{0.54}$/InP-based single-QW structure, as it depends on the well layer width c, calculated by the nonparabolic envelope function and the empirical pseudopotential methods. The absolute errors (thick solid lines) can be read on the right vertical axis.

where const simply accounts for the fact that the reference point for measuring the potential $U_{\rm fin}(z)$ is arbitrary. To take advantage of the full span of the potential offered by the chosen basis alloys one should take const$=|U_{f\min}|$, where $U_{f\min}$ denotes the minimum value of the potential in Fig. 3, equal to -120 meV; therefore

$$x'(z)=\frac{U_{\rm fin}(z)+|U_{f\min}|}{U_{0\,\max}}. \tag{39}$$

Since the graded alloy $(Q_2)_{x'}(Q_1)_{1-x'}$ is of the same quaternary type as the two basis alloys, i.e., $Ga_{x(z)}In_{1-x(z)}P_{y(z)}Sb_{1-y(z)}$, the mole fractions $x(z)$ and $y(z)$ may be written as $x(z)=x_2x'(z)$ and $y(z)=1+(1-y_2)x'(z)$. Their profiles, corresponding to the finally optimized potential of Fig. 3, are given in Fig. 4.

The purpose of this example was to illustrate the capability of BCS-based structures to extend the range of photon energies that may be used for SHG under double-resonant (intersubband) conditions. One may want, however, to find what may loosely be called ''figure of merit,'' i.e., to compare the nonlinearity provided by BCS's against that of classical barrier-confined structures at the same value of pump photon energy (allowing also for the fact that the classical structure may be only fictitous, i.e., not realizable for larger energies). For this purpose we have generated, via the supersymmetric transform, the optimized asymmetric potential starting from the idealized (not truncated) parabolic potential $U(z)=\frac{1}{2}m^*(\Delta E/\hbar)^2z^2$, keeping the same values of $\Delta E=242$ meV and $m_0=0.073$ as above. Here we found $\lambda_{\rm opt}=0.12$ and $\Pi^{(2)}_{\rm max}\approx 1000$ Å^3. This indicates that Bragg confinement is not as effective as the conventional barrier confinement and BCS wave functions have a lower overlap (hence also smaller matrix elements). However, this is the price to be paid for increasing the photon energies to a range that cannot be covered by conventional structures. Some improvement may be achieved by further optimizing the potential, via an iterated supersymmetric transform, but since the derived potentials will become even deeper, not much is to be expected of this and such a procedure was not attempted here.

Finally, we briefly discuss a point that seems relevant to justify the accuracy of the results presented. In view of the rather large energies associated with Bragg-confined states (these may be well above the barrier top and very high above the conduction-band edge of the well semiconductor) one may doubt whether even the energy-dependent effective mass gives a reasonably accurate description of the conduction-band dispersion. The problem may be circumvented by employing a more elaborate model, e.g., the empirical pseudopotential method. Such an approach would be purely numerical, more time consuming, and also difficult to implement for complicated structures such as BCS's. To resolve this point we made test calculations, using the empirical pseudopotential method, for a simple structure tractable by it: a single QW. The method is described in Ref. 22 and the form factors were taken from Ref. 23 for InP and Ref. 24 for GaP, GaSb, and InSb. Along with the ''normal'' $Ga_{0.83}In_{0.17}P_{0.46}Sb_{0.54}$/InP QW with $U_0=580$ meV, a fictitous structure with U_0 deliberately increased to 880 meV was also considered in order to access the energy range above 580 meV, where Bragg-confined states will be found in the normal structure. Bound-state energies obtained by the pseudopotential calculations were then compared against those found from the envelope-function model with nonparabolicity. Results are displayed in Fig. 5. Clearly, although the energy-dependent effective mass is definitely not the best model for the conduction-band dispersion, errors introduced by it are very low for energies less than 400 meV for QW's ~ 40 Å wide (as corresponds to our optimized BCS). At higher energies the absolute error tends to increase, but is still acceptable for all energies of interest (departures from the levels' equidistance that are within the linewidth, typically $\leqslant 10$ meV, are tolerable). Certainly, the errors introduced by the envelope-function model with nonparabolicity may also be corrected by additional polishing of the optimized potential, as described above, if it is really necessary.

As a final remark, we should note that the (GaIn)(PSb) alloy is not technologically common and there may appear difficulties if one attempts a realization of the structure proposed above. Essentially, it was chosen here to make the

calculations easier and to illustrate the idea of using BCS's for shorter-wavelength SHG while satisfying some fundamental requirements for quantum heterostructures (the lack of strain in the first place). From a practical point of view it may actually be advantageous to use other, much more studied alloys, such as the $Ga_{0.47}In_{0.53}As/Al_{0.48}In_{0.52}As$ pair, lattice matched to InP, which has a high band offset of $U_0 \approx 500$ meV. With the band-edge effective masses of $0.043m_0$ and $0.073m_0$ and band gaps of 0.87 eV and 1.49 eV, respectively, there is peculiarity of this system in that the nonparabolic effective masses turn out to be very close (to within a few percent) for a wide range of energies ($0-800$ meV measured from the $Ga_xIn_{1-x}As$ conduction-band edge). Taking the effective mass to be position independent though still dependent on energy would somewhat simplify the above considerations, and the structure design, because an ordinary Schrödinger equation might be used at any particular energy. However, since the constancy of the nonparabolic effective mass in the $Ga_xIn_{1-x}As/Al_yIn_{1-y}As$ system is only approximate, the analytically designed structure would require some amount of numerical polishing in order to restore the levels equidistance required for its application.

IV. CONCLUSION

The method for electronic-structure calculation in Bragg-confined structures with an asymmetric perturbation layer, based on the envelope-function approach, is described. It is then used to design a structure suitable for double-resonance intersubband second-harmonic generation at pump photon energies that cannot be covered by conventional QW structures. The structure is optimized by employing the supersymmetric quantum-mechanics approach, allowing for a systematic search of the best potential shape, which provides the largest nonlinear susceptibility.

*Electronic address: indjin@kiklop.etf.bg.ac.yu

[1] E. Rosencher and Ph. Bois, Phys. Rev. B **44**, 11 315 (1991).
[2] C. Sirtori, F. Capasso, D. L. Sivco, A. L. Hutchinson, and A. Y. Cho, Appl. Phys. Lett. **60**, 151 (1992).
[3] P. Bois, E. Rosencher, J. Nagle, E. Martinet, P. Boucaund, F. H. Julien, D. D. Yang, and J.-M. Lourtioz, Superlatt. Microstruct. **8**, 369 (1990).
[4] Z. Ikonić, V. Milanović, and D. Tjapkin, IEEE J. Quantum Electron. **21**, 54 (1989).
[5] J. N. Heyman, K. Craig, M. Sherwin, K. Campan, P. F. Hopkins, S. Fafard, and A. C. Gossard, in *Quantum Well Intersubband Transition Physics and Devices*, edited by H. C. Liu *et al.* (Kluwer Academic, Dordrecht, 1994), pp. 467–476.
[6] F. Capasso, C. Sirtori, J. Faist, D. Sivco, S. N. G. Chy, and A. Y. Cho, Nature **358**, 565 (1992); C. Sirtori, F. Capasso, J. Faist, D. Sivco, S. N. G. Chy, and A. Y. Cho, Appl. Phys. Lett. **61**, 898 (1992).
[7] C. Sirtori, F. Capasso, J. Faist, D. Sivco, and A. Y. Cho, in *Quantum Well Intersubband Transition Physics and Devices* (Ref. 5), pp. 301–311.
[8] C. Sirtori, F. Capasso, J. Faist, and S. Scandolo, Phys. Rev. B **50**, 8663 (1994).
[9] M. Zahler, I. Brener, G. Lenz, J. Salzman, E. Cohen, and L. Pfeiffer, Appl. Phys. Lett. **61**, 949 (1992).
[10] M. Zahler, E. Cohen, J. Salzman, E. Linder, E. Maayan, and L. N. Pfeiffer Phys. Rev. B **50**, 5305 (1994).
[11] M. Zahler, E. Cohen, J. Salzman, E. Linder, and L. Pfeiffer, Solid State Electron. **37**, 1195 (1994).
[12] A very good recent review of this topic is given by F. Cooper, A. Khare, and U. Sukhatme, Phys. Rep. **251**, 267 (1995).
[13] G. Bastard, *Wave Mechanics Applied to Semiconductor-Heterostructure* (Les Editions de Physique, Les Ulis, 1990).
[14] V. Milanović and D. Tjapkin, Phys. Status Solidi B **110**, 687 (1982).
[15] H. Jones, *Theory of Brillouin Zones and Electronic States in Crystals* (North-Holland, Amsterdam, 1960).
[16] V. Milanović, Physica (Amsterdam) **121B**, 181 (1983).
[17] A. Yariv and D. Yeh, *Optical Waves in Crystals* (Wiley, New York, 1984).
[18] D. F. Nelson, R. C. Miller, and D. A. Kleinman, Phys. Rev. B **35**, 7770 (1987).
[19] M. P. C. M. Krijin, Semicond. Sci. Technol. **6**, 27 (1991).
[20] S. Tiwari and D. J. Frank, Appl. Phys. Lett. **60**, 630 (1992).
[21] *Semiconductors. Group IV Elements and III-V Compounds*, edited by O. Madelung, Landolt-Börnstein, New Series, Group 22, Vol. III, Pt. a (Springer-Verlag, Berlin, 1991).
[22] Z. Ikonić, G. P. Srivastava, and J. C. Inkson, Solid State Commun. **81**, 841 (1992).
[23] S. Zollner, U. Schmid, N. E. Christensen, and M. Cardona, Appl. Phys. Lett. **57**, 2339 (1990).
[24] S. J. Lee, T. S. Kwon, H. S. Lee, K. Nahm, and C. K. Kim, J. Phys. Condens. Matter **1**, 5001 (1989).